Pergamon

Int. J. Heat Mass Transfer. Vol. 39, No. 12, pp. 2559–2569, 1996

0017-9310/96 $15.00+0.00

0017-9310(95)00326-6

In-tube evaporation of HCFC-22 in a 9.52 mm micro-fin/smooth tube

C. S. KUO

Department of Mechanical Engineering, National Chiao Tung University, Hsinchu 300, Taiwan, Republic of China

and

C. C. WANG†

Energy & Resources Laboratories, Industrial Technology Research Institute, Hsinchu 310, Taiwan, Republic of China

(*Received* 10 *June* 1995)

Abstract—Experimental data on evaporation in a 9.52 mm diameter micro-fin tube and a smooth tube with similar tube diameter are presented. The data were taken at two different evaporation temperatures (6°C and 10°C, respectively). The mass flux was between 100 and 300 kg m^{-2} s^{-1} and the heat fluxes were between 6 and 14 kW m^{-2}. Data were presented in the form of quasi-local heat transfer coefficients and frictional pressure gradients. The effect of heat flux, mass flux and evaporation pressure on the heat transfer coefficients were also reported in this investigation. Copyright © 1996 Elsevier Science Ltd.

1. INTRODUCTION

The micro-fin tube is widely used in refrigeration and air conditioning applications due to an increased emphasis on more compact and economical heat exchangers. The tube has small fins of triangular cross section at a helix angle of approximately from 8 to 30 degrees. One of the reasons for the growing popularity of the micro-fin tube is the larger heat transfer enhancement relative to the increased pressure drop. For instance, 50–100% increases in evaporation and condensation heat transfer coefficient with only 20–50% increase in pressure drop were reported by Schlager [1]. Although numerous investigators had conducted experiments on the evaporation and condensation heat transfer characteristics for micro-fin tubings, most of the published heat transfer/pressure drop data were averaged values of the whole test section. For example, Eckels *et al.* [2] provided HCFC-22 evaporation coefficients and pressure drop at 2°C for five currently used micro-fin tube geometries. The reported evaporation coefficients were generally average value having an entering quality of 0.1 and 0.85 leaving vapor quality, and the heat flux imposed were much higher than actually encountered in practice, and the heat transfer coefficients increases with the increases of mass flux. Schlager *et al.* [1] tested three 12.7 mm outside diameter micro-fin tubes having different helix angles (15–25°), the average heat transfer coefficients in the micro-fin tubes, based on a nominal equivalent smooth tube area, were 1.6–2.2 times larger for evaporation than those in smooth tube. These previous investigators do not define the effect of heat flux. Chiang [3] reported the evaporation heat transfer coefficients for four micro-fin tubes, the heat transfer coefficients virtually increase with heat flux. Recently, Chamra and Webb [4] reported experimental data for both condensation and evaporation at the saturation temperature 24.4°C, they argue that the mechanism of evaporation and condensation are the same if the flow is operated at vapor qualities above the region where the convective effects are dominant over nucleate boiling effects for evaporation.

Most of the published data report the average heat transfer coefficient and lacks of local evaporation coefficients, and generally their heat fluxes were not in the practical range. In addition, two-phase friction factors (multipliers) were generally not reported in previous studies. Detailed discussions of the effect of heat flux on the heat transfer coefficients for a fixed vapor quality were generally not shown. In short, work still has to be done. It is well known that the local heat transfer coefficients and frictional gradient data are required to design an evaporator with precision. The key objective of the present study is to provide quasi-local heat transfer and pressure drop data of a 9.52 mm micro-fin tube. In addition, a smooth tube with similar nominal diameter were tested for comparison.

† Author to whom correspondence should be addressed.

NOMENCLATURE

A_o outside heat transfer area of the tube [m^2]
A_i nominal inside heat transfer area of the tube [m^2]
Bo boiling number, $q/G\lambda$
C constant in Chisholm correlation
C_p specific heat of water [J kg^{-1} K^{-1}]
dP_f measured two-phase frictional pressure difference [N m^{-2}]
$dP_{f,l}$ frictional pressure difference for liquid flowing alone [N m^{-2}]
$dP_{f,v}$ frictional pressure difference for gas flowing alone [N m^{-2}]
$dP_{f,lo}$ frictional pressure difference for total mixture flowing as liquid [N m^{-2}]
ΔP_a pressure drop due to acceleration [N m^{-2}]
ΔP_g pressure drop due to gravity [N m^{-2}]
ΔP_f frictional pressure drop [N m^{-2}]
D_i maximum inside diameter of the tube [m]
D_o nominal outside diameter of the tube [m]
E Enhancement factor for single phase heat transfer
f friction factor
f_l friction factor for subcooled liquid
G mass flux [kg m^{-2} s^{-1}]
g gravitation constant [N m^{-1}]
L effective heating length [m]
LMTD log mean temperature difference [K]
$\dot{m}_r$ average mass flow rate of refrigerant [kg s^{-1}]
$\dot{m}_{water}$ average mass flow rate of coolant water [kg s^{-1}]
$Nu_{Dh,s}$ Nusselt number on the annulus side
q average heat flux [W m^{-2}]
$\dot{Q}$ average heat transfer rate [W]
$Re_{Dh,m}$ Reynolds number of the annulus side for micro-fin tube, based on hydraulic diameter
$Re_{Dh,s}$ Reynolds number of the annulus side for smooth tube, based on hydraulic diameter
Re_{LO} Reynolds number for liquid flow only
Re_{eq} equivalent two-phase Reynolds number
R_f fouling resistance [W^{-1} m^2 K]
R_w wall resistance [W^{-1} m^2 K]
S suppression factor for nucleate boiling component
T_1 inlet temperature of water at annulus side [K]
T_2 outlet temperature of water at annulus side [K]
T_{sat} saturation temperature of the refrigerant [K]
ΔT temperature rise on the water coolant [K]
ΔT_1 temperature difference, $\Delta T_1 = T_s - T_1$ [K]
ΔT_2 temperature difference, $\Delta T_2 = T_s - T_2$ [K]
U_o overall heat transfer coefficient [W m^{-2} K^{-1}]
$\bar{v}$ average specific volume [m^3 kg^{-1}]
x vapor quality
X Martinelli parameter
X_{tt} Martinelli parameter for both phase evaluated as turbulent flow
Δx difference of quality.

Greek symbols

α_f single phase heat transfer coefficient in the tube side [W m^{-2} K^{-1}]
α_{NcB} nucleate boiling heat transfer coefficient [W m^{-2} K^{-1}]
α_o heat transfer coefficient on the annulus side [W m^{-2} K^{-1}]
α_i, α_{TP} inside heat transfer coefficient [W m^{-2} K^{-1}]
ρ density of refrigerant [kg m^{-3}]
λ latent heat of evaporating vapor [J kg^{-1}]
ϕ_{lo}^2 two phase friction multiplier based on total mixture flowing as liquid
ϕ_v^2 two phase friction multiplier for vapor flowing alone
μ dynamic viscosity of refrigerant [N s m^{-2}].

Subscript

ave average value
1 inlet
2 outlet
l liquid phase
i inside
in inlet
o outside
out outlet
smooth smooth tube
tp two-phase
v vapor phase
w wall
water water.

2. EXPERIMENTAL APPARATUS

The schematic of the experimental apparatus is depicted in Fig. 1(a). The test rig is composed of three independent flow loops: namely, a refrigerant loop, a heating water flow loop and a glycol flow loop. The refrigerant flow loop consists of a variable speed gear pump which can provide refrigerant mass fluxes ranging from 50 to 500 kg m^{-2} s^{-1}. A very accurate mass flowmeter is installed between the refrigerant pump and the preheater, such that the accuracy of the mass flowmeter is generally 0.3% of the test span. The subcooled refrigerant liquid was heated in the preheater to achieve a prescribed evaporator inlet quality, and went into the test section to vaporize. Finally, the two-phase refrigerant was condensed in a shell-and-coil condenser. The horizontal test section is a double-pipe heat exchanger with effective heat transfer length 1.3 m, as shown in Fig. 1(b). Note that a preheater (also a double-pipe heat exchanger) installed at the upstream of the test section was connected to the test section by a U-bend. A 50-mm thick rubber insulation is wrapped around the double-pipe heat exchangers to ensure heat loss to the ambient to be less than 20 W for the test tube. As seen from Fig. 1(b), inside the double-pipe heat exchanger, water flows countercurrently in the test section annulus, while refrigerant is evaporated inside the test tube. The pressure drop of the refrigerant across the test tube was measured by a differential pressure transducer with 10 Pa precision. Two magnetic flowmeters, calibrated in advance with an accuracy of 0.002 l s^{-1}, were used to record the flowrates of water in the annulus of the preheater and the test section. Two absolute pressure transducers were installed at the inlet and exit of the test section with resolution up to 0.1 kPa. During each experiment, the heat flux in the test section is maintained at a desired constant value. The refrigerant leaving the test section was condensed and subcooled by a glycol circuit. The inlet temperature of the glycol is controlled by a 15 kW low-temperature thermostat.

Experiments were conducted using a commercially

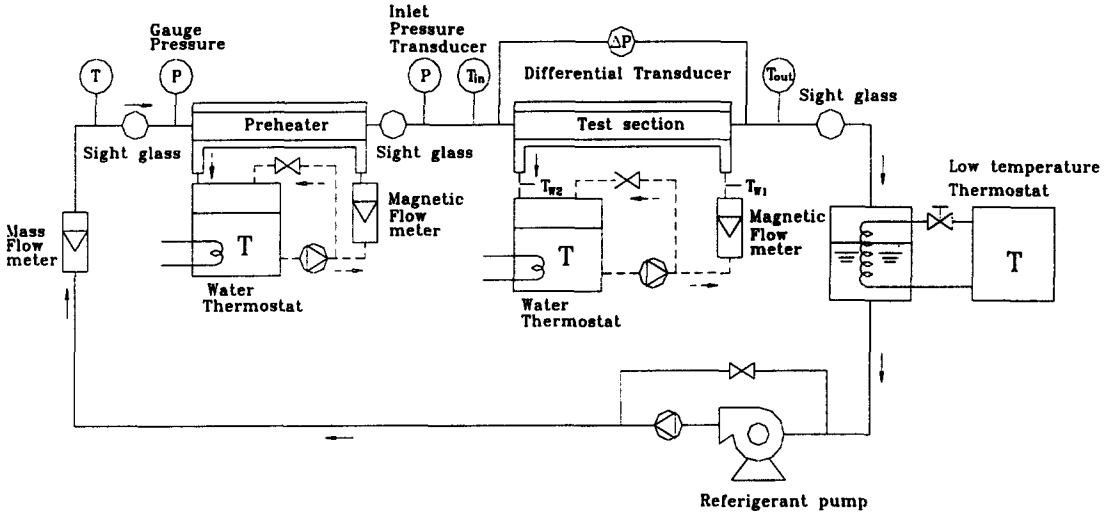

Fig. 1(a). Schematic of test loop.

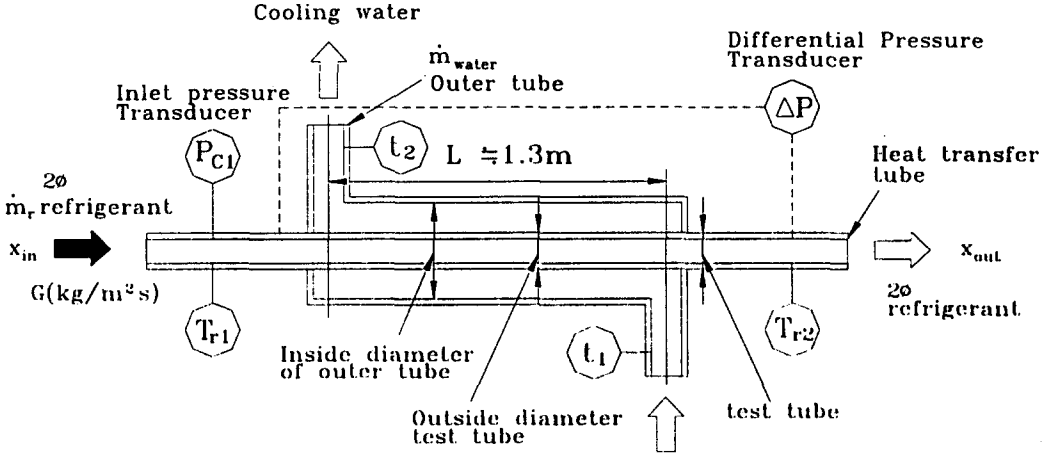

Fig. 1(b). Schematic diagram of the evaporation test section.

Table 1. Geometrical parameters of the test tubes

Tube type	Outside diameter (o.d.) [mm]	Maximum inside diameter (i.d.) [mm]	Root wall thickness (TF) [mm]	Fin height (H) [mm]	Helix angle	Number of fins (N)	Inside surface area [$m^2\ m^{-1}$]	Tube length [mm]
Smooth	9.52	7.92	0.8	...	—	—	—	1300
Micro-fin	9.52	8.92	0.3	0.2	18	60	0.044	1300

available 9.52 mm micro-fin tube and a smooth tube with identical outside diameter, the geometrical parameters of the test tubes are given in Table 1. A close-up of the test tube is also depicted in Fig. 2(a). As seen, the present micro-fin tube exhibits a slightly double enhancement [bi-direction as shown in Fig. 2(a)] as compared to conventional micro-fin tube [Fig. 2(b)]. Tests were conducted at two evaporation temperatures, namely 6 and 10°C. All of the water and refrigerant temperatures, were measured by RTDs (Pt100Ω) having a calibrated accuracy of 0.05°C. All of the data signals were collected and converted by a data acquisition system (Hybrid recorder). The data acquisition system then transmits the converted signals through GPIB interface to a host computer for further operation. Uncertainties of the heat transfer coefficients and friction factors reported in the present investigation, following the single-sample analysis proposed by Moffat [5], are tabulated in Table 2.

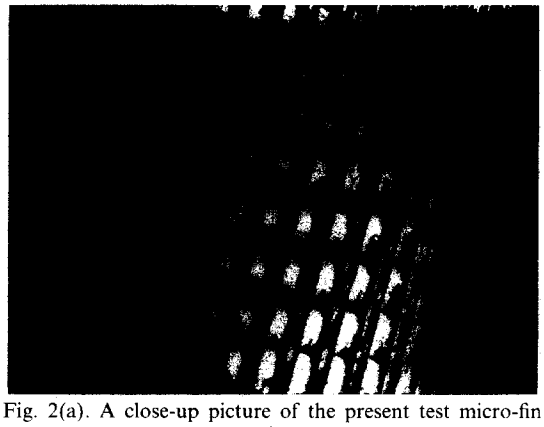

Fig. 2(a). A close-up picture of the present test micro-fin tube.

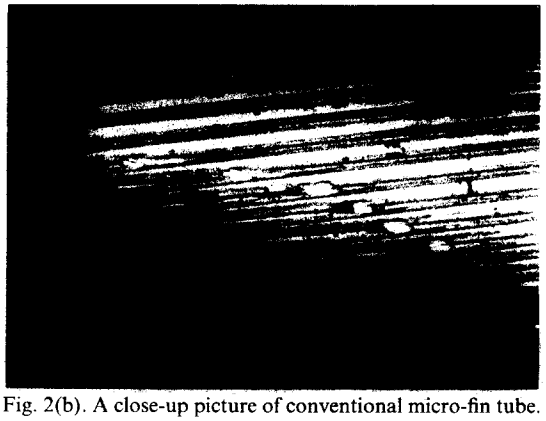

Fig. 2(b). A close-up picture of conventional micro-fin tube.

3. DATA REDUCTION FOR HEAT TRANSFER DATA

The heat duty for the test section was obtained from the flow rate and temperature drop of the water in the annulus according to the relation

$$Q = \dot{m}_{\text{water}} C_p \Delta T. \tag{1}$$

The overall heat transfer coefficient was then computed from

$$U_o = \frac{\dot{Q}}{\text{LMTD} \times A_o} \tag{2}$$

where

$$\text{LMTD} = \frac{\Delta T_1 - \Delta T_2}{\ln\left(\frac{\Delta T_1}{\Delta T_2}\right)} \tag{3}$$

$$\Delta T_1 = T_{\text{sat}} - T_{\text{water,out}} \tag{4}$$

$$\Delta T_2 = T_{\text{sat}} - T_{\text{water,in}} \tag{5}$$

where T_{sat} is the saturation temperature of the refrigerant in the test section while $T_{\text{water,in}}$ and $T_{\text{water,out}}$ denote the inlet and outlet temperature of the water coolant on the annulus. The in-tube heat transfer coefficient was obtained from the thermal resistance equation

$$\frac{1}{U_o A_o} = \frac{1}{\alpha_o A_o} + R_f + R_w + \frac{1}{\alpha_i A_i} \tag{6}$$

where α_o and α_i represent the average outside and inside heat transfer coefficients, and R_f and R_w denote fouling and wall resistance, respectively. In the present calculation, the overall resistance is based on the outer surface area, which is evaluated as $\pi D_o L$, where D_o is the outside diameter of the test tube and L is the effective heat transfer length. The properties on the water side were calculated using average temperature of inlet and outlet bulk fluid temperatures. Note that the heat transfer coefficient is based on maximum inside surface area ($\pi D_i L$) and the heat flux is based on nominal outside surface area ($\pi D_o L$). The determination of the inside heat transfer coefficient, α_i, requires knowledge of the outside heat transfer coefficient, α_o. This was accomplished by means of separate water-to-water tests on the same apparatus,

Table 2. Summary of estimated uncertainties

Primary measurements		Derived quantities		
Parameter	Uncertainty	Parameter	Uncertainty $G = 100$ kg m^{-2} s^{-1}	Uncertainty $G = 300$ kg m^{-2} s^{-1}
$\dot{m}_r$	0.3–1%	G	1.1%	0.5%
$\dot{m}_{water}$	0.5%	Re_i	0.6%	0.6%
ΔP	0.5%	f_{tp}	±9.3%	±5.6%
T	0.05°C	α	±9.4%	±12.4%

with subsequent Wilson-plot analyses yielding the individual heat transfer coefficient relationships. Figure 3 depicts the Wilson plot results of the heat transfer coefficients in the annulus for both smooth and micro-fin tubes. The Nusselt numbers on the annulus side are given by:

$$\text{Smooth tube,} \quad Nu_{Dh,s} = 0.022 Re_{Dh,s}^{0.79} Pr^{0.3} \tag{7}$$

$$\text{Micro-fin tube,} \quad Nu_{Dh,s} = 0.0206 Re_{Dh,s}^{0.8} Pr^{0.3}. \tag{8}$$

The vapor quality entering the test section (x_{in}) is calculated from the energy balance of the preheater and the quality change in each test section is given by the energy balance

$$\Delta x = \frac{\dot{Q}}{\dot{m}_r \lambda} \tag{9}$$

and the average quality in each test section is given by

$$x_{ave} = x_{in} + \frac{\Delta x}{2}. \tag{10}$$

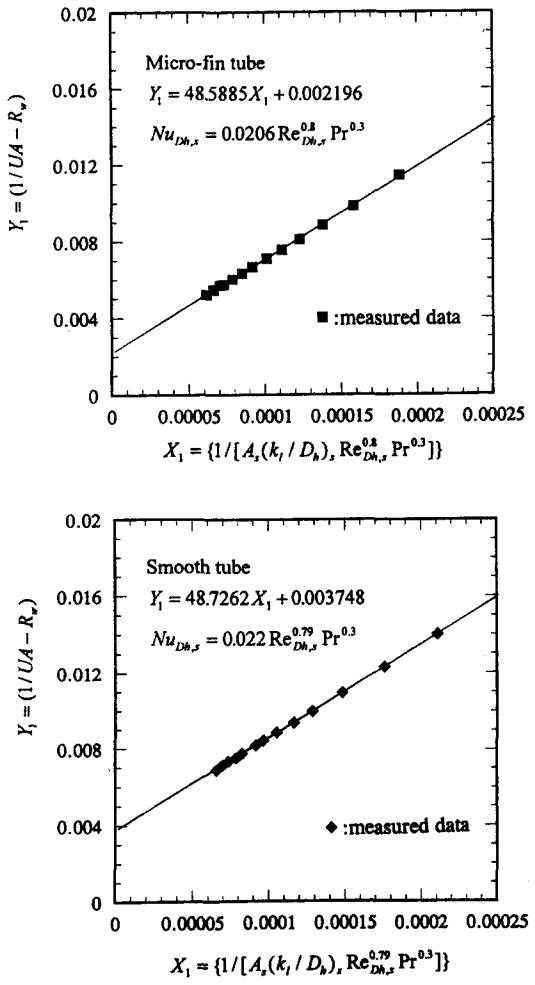

Fig. 3. Wilson plot result for the annulus heat transfer coefficient.

4. DATA REDUCTION FOR PRESSURE DROP DATA

The pressure drop data were obtained in two ways, one with heat addition and the other for adiabatic flow. For adiabatic flow, the pressure drop components for the horizontal test section include friction Δp_f, entrance Δp_i and exit Δp_e defined by

$$\Delta p = \Delta p_f + \Delta p_i - \Delta p_e. \tag{11}$$

For evaporation flows, additional pressure drop due to acceleration, Δp_a, must be included in equation (11). Estimation of the Δp_e and Δp_i are taken from Idelchik [6]. In the present investigation, the pressure loss of the connection tube and the test tubes are less than 2% as compared to the total pressure loss. Hence, uncertainties associated with evaluation of the entrance and exit losses are quite small. The frictional pressure gradient data were analyzed using the concept of the two-phase multiplier. Adiabatic experiments were conducted for easier obtaining the frictional multiplier (Δp_a can be neglected). The original multipliers are defined by:

$$\phi_v^2 = \frac{dP_f/dz}{dP_{f,v}/dz} \tag{12}$$

$$\phi_{lo}^2 = \frac{dP_f/dz}{dP_{f,lo}/dz} \tag{13}$$

where dP_f is the measured two-phase frictional pressure gradient and $dP_{f,v}$ and $dP_{f,lo}$ are the frictional pressure gradients corresponding, respectively, to the cases of vapor flowing alone in the channel and the total mixture flowing as a liquid. The multiplier typically plotted vs vapor quality x or the Martinelli parameter X, where

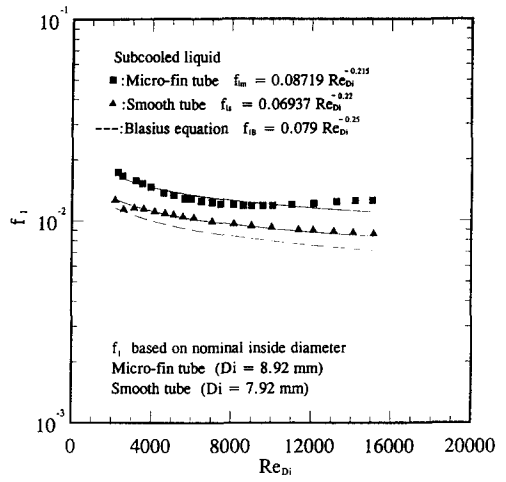

Fig. 4. Subcooled liquid friction factors in smooth and micro-fin tubes.

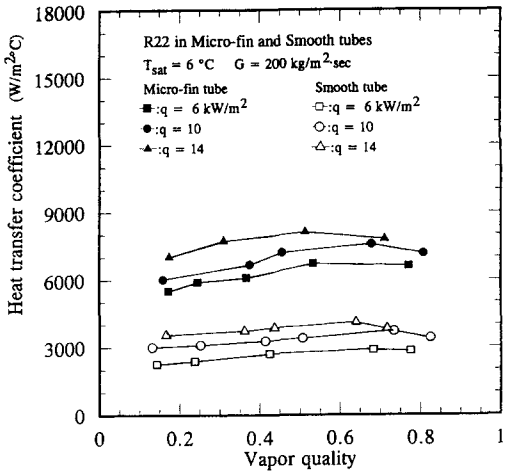

Fig. 6. Effect of heat flux on the evaporating heat transfer coefficient.

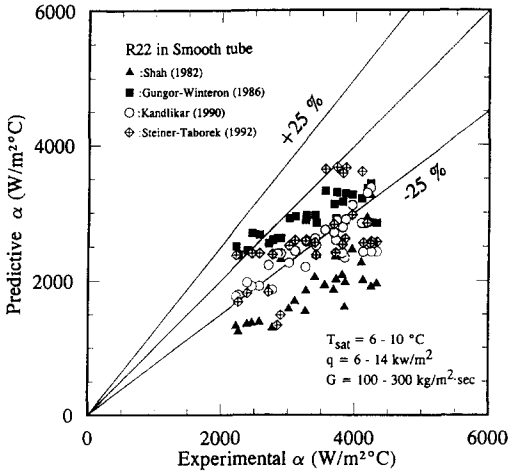

Fig. 5. Comparison of the experimental heat transfer coefficient with other heat transfer correlations (Shah [7], Gungor and Winterton [8], Kandlikar [9] and Steiner and Taborek [10]).

$$X = \sqrt{\frac{(dP_{f,l}/dz)}{(dP_{f,v}/dz)}}. \quad (14)$$

To obtain the Martinelli parameter X, it is necessary to obtain the friction factor of single-phase liquid flow. Figure 4 shows f_i *vs* Re_{Di} for the tested tubes. The base line is the Blasius friction factor equation ($0.079\ Re_{Di}^{-0.25}$). The lowest experimental $Re_{Di} \approx 2300$. The friction factors for the smooth and the micro-fin tubes are approximately 13% and 45% higher, respectively, than those predicted by Blasius equation. The curve fitted equations were also depicted in Fig. 4.

5. RESULTS AND DISCUSSION

5.1. *Heat transfer result*

The evaporation heat transfer coefficient and pressure drop data were taken at 6°C and 10°C over a mass flux range of 100 kg m^{-2} s^{-1} to 300 kg m^{-2} s^{-1}. Figure 5 shows the heat transfer results for the smooth tube as compared to the correlations of Shah [7], Gungor and Winterton [8], Kandlikar [9] and Steiner and Taborek [10]. As seen, the Shah correlation [7] underpredicts the present data for more than 40%, and the Gungor and Winterton [8] correlation gives the best agreement with the present data. Note that, all of the correlations presented in Fig. 5 somewhat under-estimated heat transfer coefficients since the data bank used were generally for larger diameters. The experimental data from Tsuchida *et al.* [11] also support this phenomenon.

Figure 6 shows the variation of heat transfer coefficient vs quality with a fixed mass flux and varying heat flux (G = 200 kg m^{-2} s^{-1}, T_{sat} = 6°C, q = 6, 10 and 14 kW m^{-2}, respectively). The test results of a smooth tube with an identical nominal outside diameter are also included in Fig. 6. As expected, the heat transfer coefficients increase with the heat flux, and our measurements show that the heat transfer coefficient for evaporation is approximately proportional to $q^{0.24}$, similar to that reported by Chiang [3] for a 10 mm helical micro-fin tube with evaporation heat transfer coefficient being proportional to $q^{0.22}$. The evaporation heat transfer coefficients for both micro-fin and smooth tube show a mild variation as quality changes. Schlager *et al.* [1] showed that the enhanced factor (α_i/α_{smooth}) is in the range 1.5–2. The experimental data for the present micro-fin tube shows an enhanced level of 2.2, and the enhanced level does not change with the heat flux in the test range. Figure 7 shows the detailed comparison of the enhanced level of the tested micro-fin tube as compared to its smooth tube counterpart. As seen, the enhanced level does not change with the mass flux, and the enhanced factor is approximately equal to 2.2.

Figure 8 shows the strong effect of mass flux on the tube performance. For a prescribed heat flux (q = 10 kW m^{-2}), the heat transfer coefficients increase with mass flux. This result is similar to the previous studies as depicted by Eckel [2]. One can find from the exam-

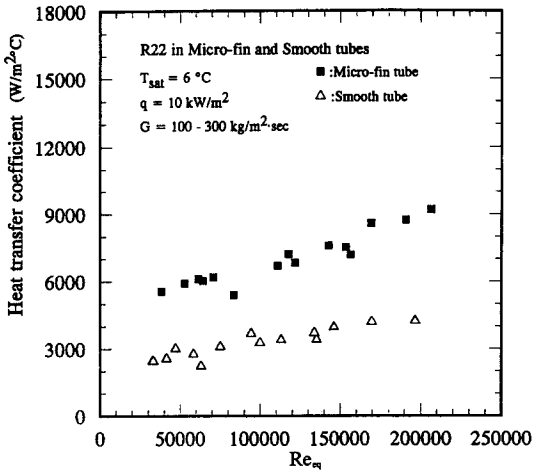

Fig. 7. Heat transfer coefficients vs Re_{eq} for both smooth tube and micro-fin tube.

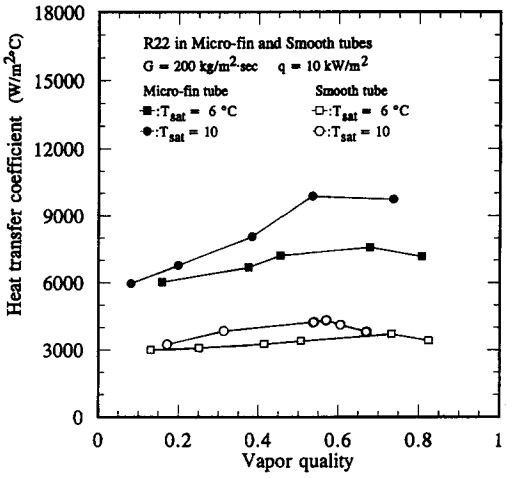

Fig. 10. Effect of evaporating temperature on the heat transfer coefficient.

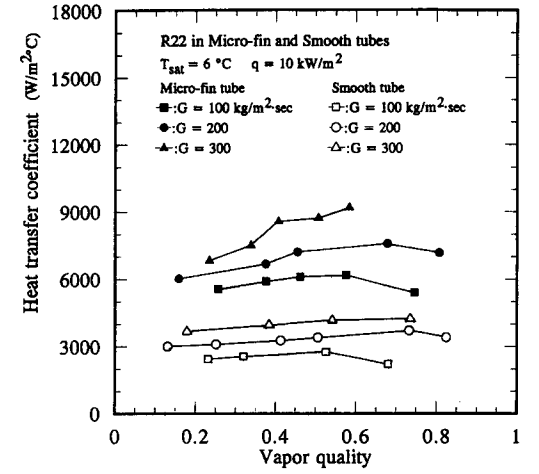

Fig. 8. Effect of mass flux on the evaporating heat transfer coefficient.

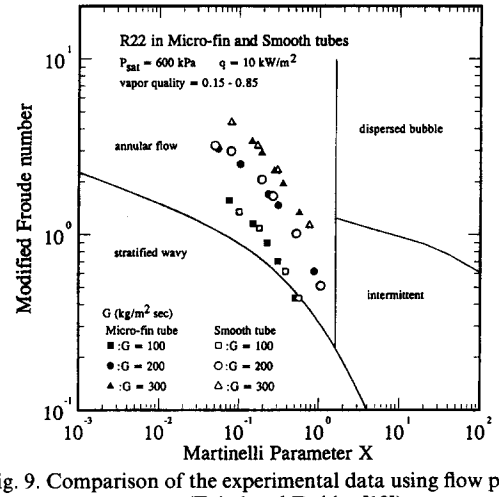

Fig. 9. Comparison of the experimental data using flow pattern map (Taitel and Dukler [12]).

ination of the data point using the flow pattern map (Fig. 9) proposed by Taitel and Dukler [12] that, for lower mass flux $G = 100$ kg m^{-2} s^{-1}, the flow regions for the tested data were in the stratified wavy region or close to the margin between the annular and stratified flow region. As a result, a smaller heat transfer coefficient is expected and the data indicate that no significant changes of heat transfer coefficients occur. For a higher mass flux, $G = 300$ kg m^{-2} s^{-1}, the flow pattern for the test data were found to be in the annular flow region, and therefore, higher heat transfer coefficients are expected.

The effect of evaporation temperature on the heat transfer coefficients were illustrated in Fig. 10. As shown, the heat transfer coefficients increase with the evaporation temperature at high quality region ($x > 0.2$). However, the evaporation temperature does not affect the heat transfer coefficients for $x < 0.2$. Note that the smooth tube also reveals a similar trend. This can be illustrated from the correlation developed by Gungor and Winterton [8] as

$$\alpha_{TP} = E\alpha_f + S\alpha_{NcB} \tag{15}$$

where

$$E = 1 + 24000Bo^{1.16} + 1.37(1/X_{tt})^{0.86} \tag{16}$$

$$S = \frac{1}{1 + 0.00000115E^2 Re_l^{1.17}}. \tag{17}$$

Since heat flux is held constant, the boiling number, Bo, is constant for a prescribed heat flux. X_{tt} decreases with the increase of vapor quality. Eventually, E increases and S decreases with the vapor quality. The enhancement of heat transfer coefficient at higher quality region is due to the increase of force convection heat transfer component. On the contrary, as vapor quality decreases, E approaches a constant value for different evaporation temperature, and as a result, no detectable variation of heat transfer coefficients is found at low quality region.

5.2. *Pressure drop results*

For adiabatic conditions, the pressure drop data are to be plotted in Fig. 11. The pressure drop per unit length between pressure taps, $\Delta p/L$, increases significantly with the mass flux, and with quality. For a given quality, the pressure drop is approximately proportional to $G^{1.65}$. The influence of G on pressure drop for the micro-fin tube is somewhat lower than that of a spiral inner tube with fin geometry (15.9 mm o.d., 32 fins, fin height = 0.635 mm) tested by Kubanek and Miletti [13]. Their test results are proportional to $G^{1.71}$–$G^{1.9}$ for various qualities. In addition, the adiabatic pressure gradients for micro-fin tubes are 15–20% higher as compared to that for smooth tubes. For non-adiabatic conditions, the pressure gradient difference between micro-fin and smooth tube seems to be negligible as shown in Fig. 11. As known, the total pressure gradient for heat-addition conditions is

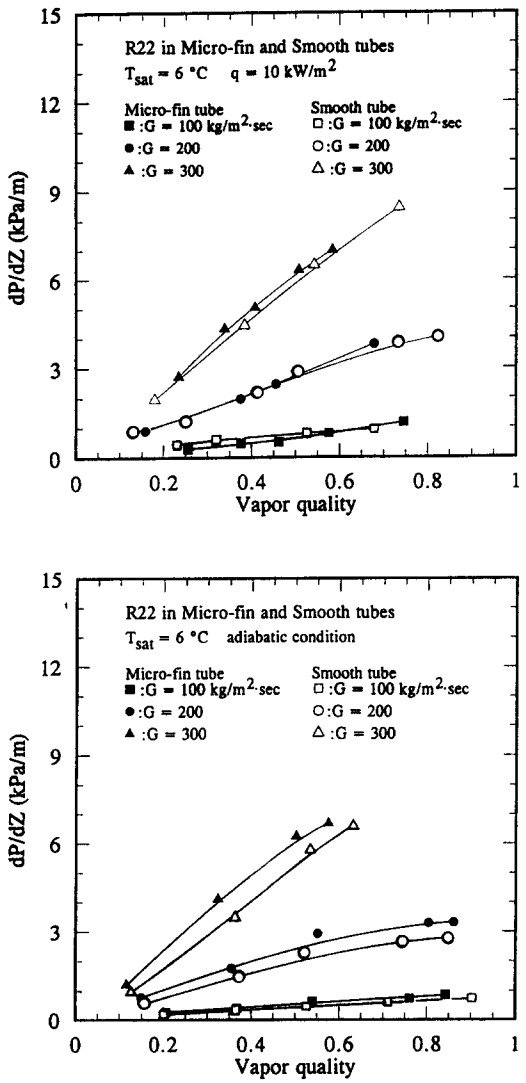

Fig. 11. Two-phase flow pressure drop in micro-fin tube and smooth tube with and without heat addition.

$$\Delta p = \Delta p_f + \Delta p_a \tag{18}$$

and

$$\Delta p_a = G^2 v_{fg} \frac{dx}{dz}. \tag{19}$$

Since the inside tube diameter for smooth tube is 10% lower than that of micro-fin tube, the refrigerant mass flowrate of smooth tube should be 20% lower than that of micro-fin tube for a given mass flux G, Δp_a for smooth tube will be approximately 20–25% higher than that of micro-fin tube. Accordingly, the difference in pressure gradient for micro-fin and smooth tube decreased with heat-addition condition.

For smooth, circular tubes, as proposed by Chisholm [14]:

$$\phi_v^2 = 1 + CX + X^2 \tag{20}$$

where X is the Martinelli parameter, and is given by equation (14), the constant C ranges from 5 to 20, depending on whether the liquid and vapor phases are laminar or turbulent and on the physical properties of the mixture. Figure 12 shows the measured data plotted in the form ϕ_v^2 vs X and that predicted by equation (20) for $C = 5$ and 20. The present results are consistent with those of Yang and Webb [15] and Wambsganss *et al.* [16] in small rectangular channel. Note that, C increases with mass flux at this low mass fluxes range. The two-phase multiplier data for each of the tested mass fluxes are compared in Fig. 13, the data deviate from a constant value. The Chisholm correlation was based on data mainly from relatively large diameter and higher mass fluxes, while the results presented here are in a practical range, such that C is a function of Martinelli parameter and mass flux. Wambsganss *et al.* [16] proposed a modification on the C factor in the Chisholm correlation as

$$C = C(X, Re_{LO}) = aX^b \tag{21}$$

where

$$a = -2.44 + 0.00939 Re_{LO} \tag{22}$$

$$b = -0.938 + 0.000432 Re_{LO}. \tag{23}$$

However, this correlation is valid for $Re_{LO} < 2000$ and can not be used to describe the present data (the Re_{LO} values in the present study are greater than 4000). Using a multi-regression process, C can be correlated as

$$C = 0.045163 X^{-0.367} Re_{LO}^{0.56}. \tag{24}$$

Equation (24) can correlate 93% of the present data within ±20%, and 61% of the data points within ±10%, as shown in Fig. 14, the C values being insensitive to the tube geometry (both micro-fin tube and smooth tube). The results here suggest that, in the smaller diameter tubes with round tube geometry, a variable C should be used instead of a constant C.

A more recent correlation developed by Friedel

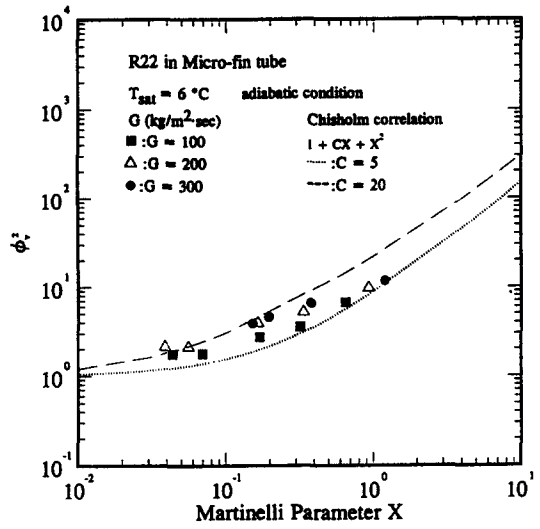

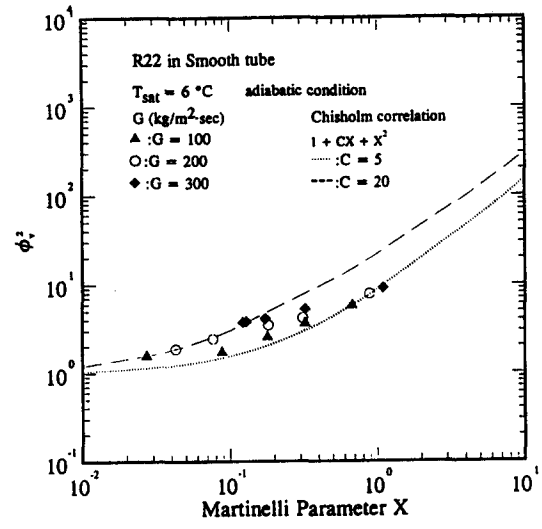

Fig. 12. Frictional multiplier vs Martinelli parameter for the experimental data.

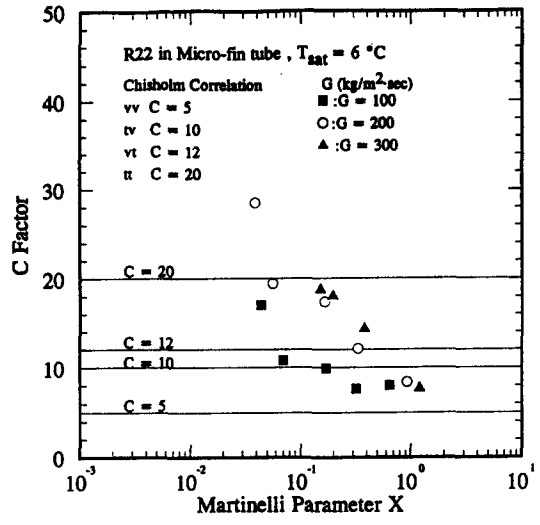

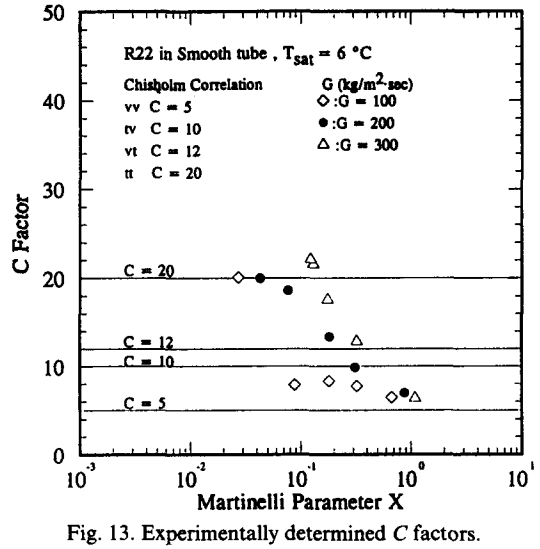

Fig. 13. Experimentally determined C factors.

[17], developed for both horizontal flow and vertical upflow with a data bank over 25 000 points, is calculated and compared with the present experimental data in Fig. 15. As seen, the Friedel correlation [17] can predict the present data for micro-fin and smooth tubes within $\pm 25\%$, but the effect of mass flux on ϕ_{lo}^2 for the present data is not consistent. This is because of the fact that the Friedel correlation [17] is more appropriate for larger diameter and larger mass flux. Nonetheless, our experimental data is consistent with Wambsganss *et al.* [16] in small mass flux range ($G < 400$ kg m^{-2}).

An alternative approach to reduce the two-phase friction data is to introduce the two-phase friction factor, f_{tp}, using a mean two-phase viscosity, $\bar{\mu}$, in the normal friction factor relationship, the two-phase friction factors can be expressed as

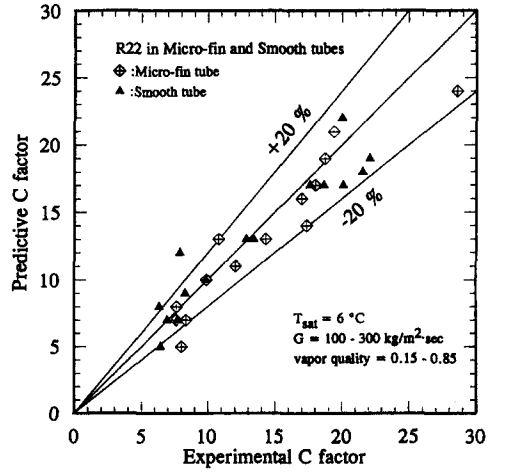

Fig. 14. Comparison of the modified C predictions and the experimental data.

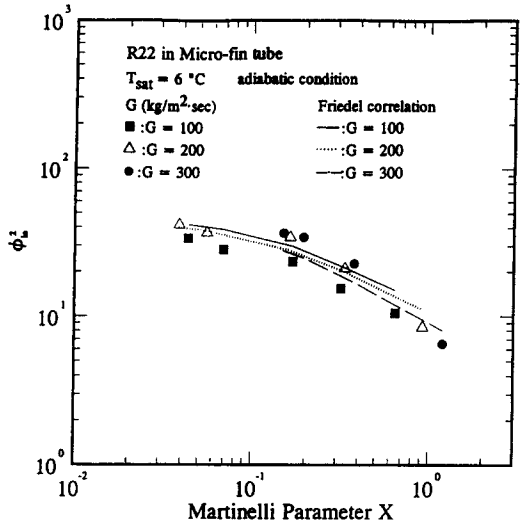

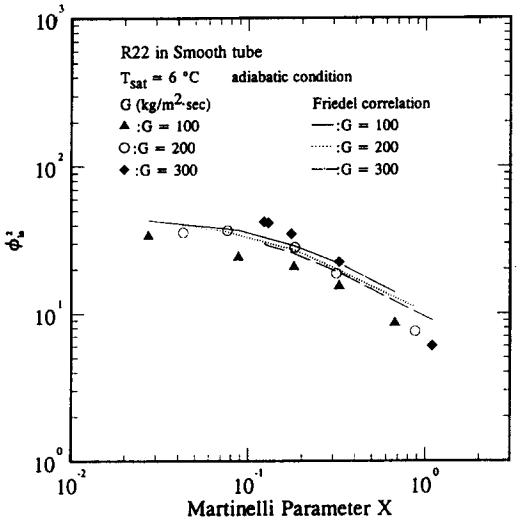

Fig. 15. Comparison of two-phase multiplier predicted by Friedel with experimental data.

$$\left(\frac{dP}{dz}\right)_f = \frac{2f_{tp}G^2\bar{v}}{D_i} \tag{25}$$

and

$$\bar{v} = xv_v + (1-x)v_l \tag{26}$$

$$\bar{\mu} = \bar{\rho}[(xv_v\mu_v + (1-x)v_l\mu_l)] \tag{27}$$

$$Re_{eq} = \frac{GD_i}{\bar{\mu}}. \tag{28}$$

Figure 16 shows the two-phase friction factors defined by equation (25) plotted against Re_{eq} for both smooth and micro-fin tubes. The mean two-phase viscosity is taken from Dukler *et al.* [18]. The figure shows a very small dependence of the friction factor on Reynolds number. Similar results were reported by Yang and Webb [15] in their rectangular conduit. The present

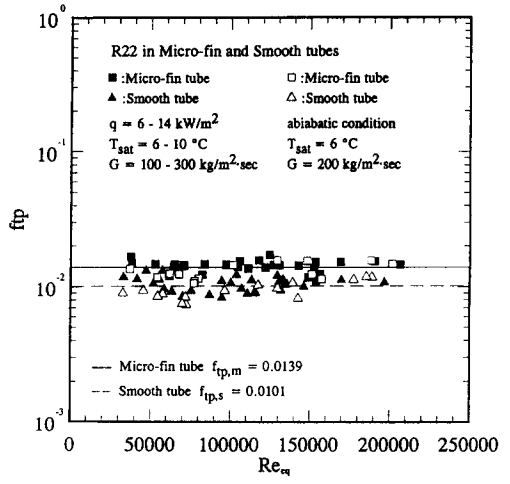

Fig. 16. Two-phase flow friction factor in smooth and micro-fin tube.

experimental data suggest $f_{tp,s} \approx 0.0101$ for smooth tube and $f_{tp,m} \approx 0.0139$ for micro-fin tube.

6. CONCLUSIONS

Experimental data on evaporation in a 9.52 mm micro-fin and its corresponding smooth tube are presented. The experimental data were taken at two different evaporation temperatures (6°C and 10°C), the range of mass flux is between 100 and 300 kg m^{-2} s^{-1} and the heat flux varies from 6 to 14 kW m^{-2}. Data were presented in the form of quasi-local heat transfer and frictional pressure gradient. The effect of heat flux, mass flux and pressure on the heat transfer coefficient are reported in the present investigation. The heat transfer coefficient increases with heat flux, mass flux and evaporation temperature. The heat transfer enhancement ratio, in the present investigation, for the micro-fin tube is approximately equal to 2.2.

The Friedel correlation [17] can predict the two-phase friction multiplier for both smooth tube and micro-fin tube with success. It is also suggested that a modification of the Chisholm correlation [14] can be used instead of a constant C value. The two-phase friction factors are found to be insensitive to the Reynolds number.

Acknowledgements—The authors would like to express gratitude for the Energy R&D foundation funding from the Energy Commission of the Ministry of Economic Affairs, which has made this study possible. Suggestions from Prof. Ralph Webb were very appreciated.

REFERENCES

1. L. M. Schlager, M. B. Pate and A. E. Bergles, Evaporation and condensation heat transfer and pressure drop in horizontal, 12.7-mm micro-fin tubes with refrigerant 22, *J. Heat Transfer* **112**, 1041–1045 (1990).
2. S. J. Eckels and M. B. Pate, Evaporation heat transfer coefficients for R-22 in micro-fin tubes of different configurations, HTD-Vol. 202, pp. 117–125 (1992).

3. R. Chiang, Heat transfer and pressure drop during evaporation and condensation of refrigerant-22 in a 7.5 mm diameter axial and helical grooved tubes, *A.I.Ch.E. Symp. Ser.* **89**(295), 205–210 (1993).
4. L. M. Chamra and R. L. Webb, Condensation and evaporation in micro-fin tubes at equal saturation temperatures, *J. Enhanced Heat Transfer* **2,** 1–12 (1995).
5. I. E. Idelchik, *Handbook of Hydraulic Resistance*, 3rd Ed, Chaps 3 and 4. CRC Press, Florida (1994).
6. R. J. Moffat, Describing the uncertainties in experimental results, *Exp. Thermal Fluid Sci.* **1,** 3–17 (1988).
7. M. M. Shah, Chart correlation for saturated boiling heat transfer: equations and further study, *ASHRAE Trans.* **88**(1), 185–196 (1982).
8. K. E. Gungor and R. H. S. Winterton, A general correlation for flow boiling in tubes and annuli, *Int. J. Heat Mass Transfer* **29,** 351–358 (1986).
9. S. G. Kandlikar, A general correlation for saturated two-phase flow boiling heat transfer inside horizontal and vertical tubes, *J. Heat Transfer* **112,** 219–228 (1990).
10. D. Steiner and J. Taborek, Flow boiling heat transfer in vertical tubes correlated by an asymptotic model, *Heat Transfer Engng* **13,** 43–56 (1992).
11. T. Tsuchida, K. Yasuda, M. Hori and T. Otani, Internal heat transfer characteristics and workability of "THER MOFIN" tubes, *Hitachi Cable Review* (12) 59–64 (1993).
12. Y. Taitel and A. E. Dukler, A model for predicting flow regime transitions in horizontal and near horizontal gas–liquid flow, *A.I.Ch.E. Jl* **22,** 47–55 (1976).
13. G. R. Kubanek and D. L. Miletti, Evaporative heat transfer and pressure drop performance of internally-finned tubes with refrigerant 22, *J. Heat Transfer* **101,** 447–452 (1979).
14. D. Chisholm, A theoretical basis for the Lockhart–Martinelli correlation for two-phase flow, *Int. J. Heat Mass Transfer* **10,** 1767–1778 (1967).
15. C. Y. Yang and R. L. Webb, Condensation of R-12 in small hydraulic diameter extruded aluminum tubes with and without micro-fins, *Int. J. Heat Mass Transfer* **39,** 791–800 (1996).
16. M. W. Wambsganss, J. A. Jendrzejcyk, D. M. France and N. T. Obot, Friction pressure gradients in two-phase flow in a small horizontal rectangular channel, *Exp. Thermal Fluid Sci* **5,** 40–56 (1992).
17. L. Friedel, Improved friction pressure drop correlations for horizontal and vertical two-phase pipe flow, *European Two-Phase Flow Group Meeting*, Paper E2 (1979).
18. A. E. Dukler, M. Wicks and R. G. Cleveland, Pressure drop and hold up in two-phase flow-Part A. A comparison of existing correlations; Part B. An approach through similarity analysis, *A.I.Ch.E. Jl* **10**(1), 38–51 (1964).